Research Article

Research on Wind Load Calculation Based on Identical Guarantee Rate Method

Tao Ye [ID],[1,2,3] **Ledong Zhu,**[1,2] **Zhongxu Tan,**[1] **and Lanlan Li**[4]

[1]*State Key Laboratory of Disaster Reduction in Civil Engineering, Tongji University, Shanghai 200092, China*
[2]*Department of Bridge Engineering, Tongji University, Shanghai 200092, China*
[3]*China Communications Construction Second Harbor Fourth Engineering Company Ltd., Wuhu, Anhui 241000, China*
[4]*Purple Mountain Laboratories, Nanjing 210000, Jiangsu, China*

Correspondence should be addressed to Tao Ye; yetao1982827@163.com

Wind load on building surface is one of the main loads for structural design; scholars in this field have put forward some methods to calculate wind load, such as Simiu method and Kasperski method. Based on the basic theory of probability and the systematic analysis of the surrounding environment and turbulence, a random variable model for calculating wind load is established. According to the model, through the analysis of the relationship between guarantee rate and wind load, a numerical calculation method to calculate wind load is proposed based on extreme value analysis and polynomial fitting theory. To verify the performance of the algorithm, wind tunnel experiments were carried out to obtain a large number of first-hand measured data of high-rise building (Shanghai World Financial Center). Based on the measured data, the algorithm is simulated, and calculated results are analyzed, including wind pressure distribution on building and probability distribution of fluctuating wind pressure of some measuring points. The validity and accuracy of the proposed model and algorithm are verified by the comparative analysis and theoretical analysis of the calculation results.

1. Introduction

The wind load on the building surface is one of the main loads during the stage of the structure design. For high-rise buildings structure, the response caused by wind load accounts for a considerable proportion of the total load and even plays a decisive role. Accurate estimation of the wind load on the building surface envelope is critical to reducing the wind disaster loss [1, 2]. Reasonable wind-resistant design is of great significance to ensure the function of building structures. In the wind-resistant design of structures, to ensure the safety and reliability of structures, it is necessary to evaluate the extreme wind load reasonably. The extreme wind load is related to the wind characteristics and the aerodynamic characteristics of the structure. The former is in the form of wind speed, and the latter is in the form of the wind pressure coefficient. Targeting the wind-resistant design of high-rise buildings, in recent research studies,

many wind load calculation and wind pressure extremum estimation methods are proposed. Zhang [3] provides a novel wind load calculation for the structural design concerning the directionality and uncertainty effect. Xue et al. [4] proposed a novel method of identifying structural state, parameters, and unknown wind load estimation from incomplete measurements. Chowdhury et al. [5] give a better understanding of wind load effects on roof-to-wall connections of a typical low-rise gable roof residential structure subjected to combined impacts of wind and a potential breach of the building envelope. Yao et al. [6] built a joint probability density function of along-wind direction and across-wind direction on wind load effect based on the high-frequency force balance test and Copula Frank function, and taking the rule of stress, a design basis solved the combination coefficient with a certain assurance of wind load component. Zhuang et al. [7] researched the non-Gaussian features of wind pressure fluctuations on a rectangular

high-rise building when the wind was normal to the short and long edges through a wind tunnel test of the rigid model. Meng et al. [8] analyzed impacts of various parameters like turbulence model, approaching-flow speed, and grid type on wind pressure coefficients over CAARC buildings. Luo [9] regarded wind load as a function of average wind and load coefficient and analyzed the relationship among wind load, wind speed, and load coefficient. Bhattacharyya and Dalui [10] conducted a comprehensive study on the average pressure coefficient of "E" plan-shaped high-rise buildings using wind tunnel test and computational fluid dynamics (CFD) numerical simulation. Luo et al. [11] proposed a simplified formula for calculating wind pressure extremum based on Hermite polynomial and wind tunnel test data during the long sampling time intervals. Ma [12] proposed the wind pressure extremum algorithm combining the experimental data with numerical simulation. Malick et al. [13] put forward the wind pressure coefficient model of "C" plan-shaped tall building model and process of obtaining its solution. Quan et al. [14] proposed a wind pressure extreme value estimation method based on generalized extreme value theory. Quan et al. [15] proposed extreme value estimating method of non-Gaussian wind pressure.

In terms of wind load calculation, this topic has been studied a long time ago. The widely used methods include the extreme value estimation method based on the assumption that the wind pressure or the extreme wind pressure on the building surface follows a certain probability distribution [16]. Based on the Davenport method for the Gaussian process, several scholars have proposed different improvements to the calculation model and determination method of the non-Gaussian peak factor of fluctuating wind pressure. Kareem and Zhao [17] expressed the non-Gaussian process as Hermite polynomials of the Gaussian process considering higher-order statistics, thus extending the peak factor method to the non-Gaussian process. The process conversion method of Simiu and Filliben [18] uses the principle of equivalent probability to transform non-Gaussian process into Gaussian process and proposes a method for calculating the extreme value of non-Gaussian process. Simiu method [18, 19] transforms the most unfavorable annual wind load sequences into the annual equivalent wind speed sequences from the point of view of the wind pressure, where the equivalent wind speed reflects implicitly the influence of wind direction. By assuming that the annual equivalent wind speed series obeys a certain probability distribution, the wind load value with a certain return period is obtained. Kasperski and Hoxey [20–22] improved the abovementioned method and proposed a more accurate extreme value calculation method (Kasperski method). Diniz et al. method [23] is based on Monte Carlo simulation and introduces a series of factors of cognitive uncertainty to study the wind load estimation method considering wind direction more comprehensively and accurately. In their methods, the peak factor method is used to obtain the most unfavorable wind pressure coefficient extreme value under the whole wind direction, and the wind pressure coefficient time history of the actual measuring point is obtained through wind tunnel test, and the wind

load estimation value is obtained according to Bernoulli expression. The existing calculation method requires a large amount of data and calculation, a complex calculation process, but inaccurate results are obtained. Therefore, it is not suitable for engineering applications. It is valuable to design a method with "simplifying calculation and ensuring accuracy" to estimate wind pressure.

Based on the basic probability theory and combined with the systematic analysis of the surrounding environment and turbulence of buildings, a random variable model is established to calculate the wind load considering wind direction. Through the analysis of the relationship between the guarantee rate and the wind load, the "asymmetric quantile truncation method" is proposed to determine the quantile of the wind pressure extreme value. On this basis, a numerical solution for the design wind load is proposed. From the point of view of structural wind resistance design, the numerical model of wind load calculation and the design structure wind load are obtained. Taking the wind pressures on claddings of the Shanghai World Financial Center as an example, the accuracy and effectiveness of the proposed algorithm are systematically verified.

2. Wind Load Calculation Model

At present, to estimate wind pressure, researchers first use the peak factor method to calculate the most unfavorable extreme value of the wind pressure coefficient under the whole wind direction and obtain the wind speed extreme value of the annual wind speed extreme series of the whole wind direction from the meteorological data and then take the calculated quantile value corresponding to a certain guarantee rate (return period) as the design wind speed extreme value. The influence of wind direction is not considered in the above calculation of the two parameters. The calculated wind pressure coefficient and wind speed extremum are substituted into Bernoulli formula to obtain the wind pressure design value (hereinafter referred to as the traditional method). The traditional calculation method of design wind load is based on model:

$$W_{\text{des}} = \frac{1}{2}\rho \widehat{V}_{\text{des}}^2 \widehat{C}_{\text{des}}, \tag{1}$$

where W_{des} is the design wind load, $\widehat{V}_{\text{des}}^2$ is the extreme design wind speed, and $\widehat{C}_{\text{des}}$ is the extreme design wind pressure coefficient. The design extreme wind pressure coefficient can be calculated by peak factor method.

In model (1), the influence of wind direction is not fully considered, so the calculated wind load based on this model lacks the results caused by wind direction effect. In the process of calculating wind load, the probability distribution that annual wind speed discrete time history under all wind direction follows is obtained by assuming based on the original wind speed data, and then the quantile value corresponding to the specified guarantee rate is obtained, which is the extreme wind speed. For the wind pressure coefficient, their most unfavorable value under the whole wind direction is regarded as the extreme wind pressure coefficient, and the

synchronous influence caused by wind speed and wind pressure coefficient on wind load is ignored. In this way, the actual guarantee rate corresponding to the design wind load obtained is quite different from the guarantee rate that the engineering application needs to meet.

For a certain measuring point on the building surface, there are great differences in the extreme values of wind pressure under different wind directions. There are two reasons for the difference: one is that the extreme wind speeds at different wind directions are different, which is mainly related to the macro meteorology in the region, such as climate or cyclone type; the other is that the extreme wind pressure coefficients at different wind directions are different, which is mainly related to the environment around buildings and wind flow [24, 25]. The impact of wind on buildings and the surrounding environment is as follows: (1) in the area with dense high-rise buildings, the original wind field is changed by the buildings; under the same conditions, the local wind speed around the buildings increases; (2) wind load is a kind of random load, which is greatly affected by building height, wind direction, wind intensity, and duration; (3) the outer contour of a building is generally non-manifold, so the flow field is inevitably accompanied by separated flow, vortex shedding and oscillation, and even more seriously, the coupling oscillation of structure and fluid; (4) the roughness of the building surface also affects the magnitude of the wind force, and the roughness of the building surface will also increase the effect of the wind

force. The interaction between buildings and surrounding environment will be caused by wind. The shape, size, and number of buildings, the relative position of buildings, wind direction angle, wind field, and wind speed are all related to the mutual interference. The model described by formula (1) and the existing wind load calculation methods [18, 22, 23] do not fully involve these factors. In this paper, a series of factors of cognitive uncertainty are considered in the design of the algorithm model, so as to more comprehensively and accurately study the wind load estimation method considering wind direction, in which a series of factors of cognitive uncertainty include the wind-induced effect in short duration τ (bending moment, shear force, and displacement), the roughness degree z_0 of the representative landform of the upwind location of the building, the wind speed conversion factor u, the wind speed v, the site type γ, shape coefficient Tx and wind pressure point correlation coefficient r, local shape coefficient of wind pressure μ_p, and variation of wind pressure coefficient. With the progress of technique for the measurement of unsteady aerodynamic force [26], wind pressure distributions and unsteady aerodynamic characteristics are investigated and analyzed [27], and the local aerodynamic force coefficient [28] plays an important role in studying the characteristics of unsteady aerodynamic forces acting on a structure. Based on the above analysis, the obtained wind load calculation model is more comprehensive than (1). The wind load model proposed in this paper is given by

$$W_{\text{des}} = \frac{1}{2\rho \widehat{V}_{\text{des}}^2(v, \theta_i, h) \widehat{C}_{\text{des}}(z_0, \theta_i, h, \gamma, r, u(\theta_i, h), C, \mu_p/C_p)}, \quad i = 1, \ldots, N, N \text{ is number of wind angles}, \tag{2}$$

where W_{des} is the design wind load, $\widehat{V}_{\text{des}}^2$ is the extreme design wind speed related to wind angle θ_i, and $\widehat{C}_{\text{des}}$ is the extreme design wind pressure coefficient related to wind angle θ_i. C is the aerodynamic force coefficient. μ_p/C_p is the local shape coefficient of wind pressure related to coherence of wind pressure.

The algorithm proposed in this paper is based on the above model to calculate the wind load with the premise of uniform guarantee rate, so as to ensure a more safe and economical design.

3. Calculation of Wind Load Based on an Identical Guarantee Rate

3.1. Algorithm Overview. The random variables in the model (2) follow the nonlinear distribution, and the calculation of wind load based on this model involves the calculation of the square and product of random variables. To calculate the wind load according to model (2), it is necessary to solve the calculation problem of nonlinear random variables, which is difficult in probability theory. In addition, due to the complexity of wind field disturbance, it is difficult to find a certain probability distribution that wind pressure time history follows, which is not conducive to the application of

practical engineering. Therefore, the numerical calculation method not only obtains the required wind load results, but also meets the accuracy requirements. This paper proposes a discrete numerical calculation method to get wind load. Based on the analysis of the relationship between guarantee rate and wind load, the "asymmetric quantile truncation method" is used to calculate the wind load related to a specific guarantee rate, and the maximum and minimum wind load sequences are obtained. Then, the required design wind load is calculated by using the algorithm proposed in this paper. Figure 1 is the schematic diagram of the algorithm model proposed in this paper.

3.2. Determination of Asymmetric Quantile. In order to solve the aforementioned nonlinear probability model and calculate the wind load value in the model, a bilateral guarantee rate model is proposed in this paper. The wind pressure time history of high-rise building envelope surface is mostly non-Gaussian distribution, and there is a one-to-one correspondence between a specified guarantee rate and its corresponding peak factor. Therefore, the bilateral guarantee rate model can be determined according to the maximum sequence $\widehat{C}_P$ and minimum sequence C_P of wind pressure
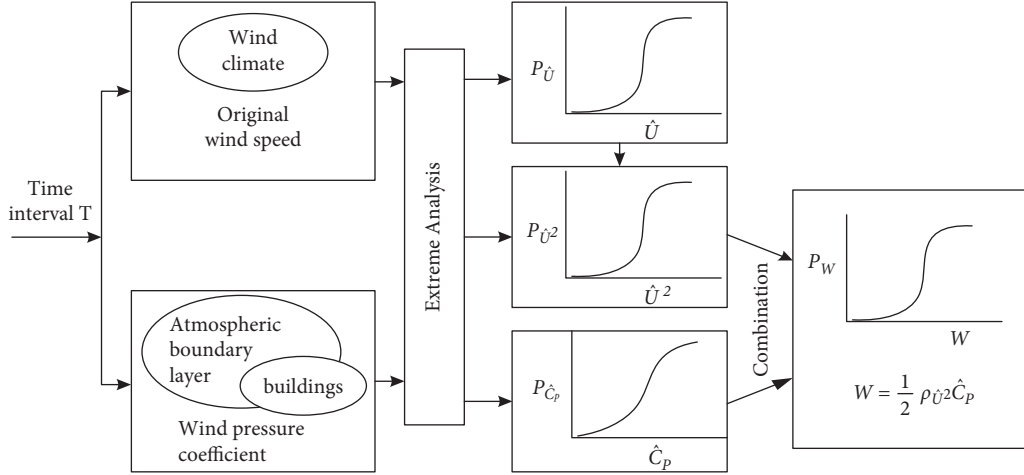
FIGURE 1: Modeling diagram for calculating wind load.

time history. The guarantee rate corresponding to a quantile between the positive and negative extreme wind pressure coefficients symmetrical to the mean value is P_{fix}. It is defined as follows:

The establishment process of the model can be seen in Figure 2, and the model can be expressed by

$$P\left\{\widehat{C}_P\right\} - P\left\{\overset{\vee}{C}_P\right\} = P_{\text{fix}}, \tag{3a}$$

$$f(k) = P\{C_{P\text{mean}} + k \cdot C_{P\text{rms}}\} - P\{C_{P\text{mean}} - k \cdot C_{P\text{rms}}\} - P_{\text{fix}} = 0, \tag{3b}$$

where k is the peak factor, while $C_{P\text{mean}}$ and $C_{P\text{rms}}$ are the mean pressure coefficient and root mean square of the fluctuating pressure coefficient, respectively. This algorithm is based on analyzing the relationship between the guarantee rate and wind load. In general, the corresponding guarantee rates for 50 years and 100 years are 98% and 99%, respectively ($P = 1 - 1/T$), and the corresponding guarantee rate for 1000 years is 99.9%. The principle of the algorithm is illustrated by taking the guarantee rate of 98%. When the guarantee rate is 98%, the right quantile of the extreme wind pressure probability density curve in Figure 3 is the wind pressure extreme value corresponding to probability 99%, and the left quantile is the extreme value of wind pressure corresponding to a probability of 1%.

In the calculation process described below, the calculation symbols are defined as follows:

$W_{99\%}$: extreme design wind load at quantile (value is 99%) on the right side

$W_{1\%}$: extreme design wind load at the quantile (value is 1%) on the left side

For a single random variable, there are four cases of the probability distribution and location quantile value in coordinate system, as shown in Table 1. The four cases correspond to Figures 3(a)–3(d), respectively:

According to the above four extreme wind pressure probability density distributions, to meet the guarantee rate
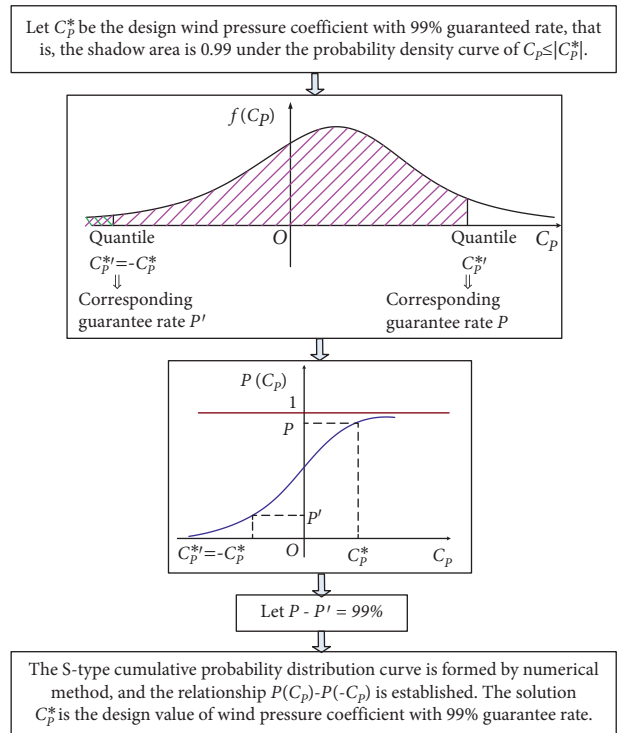

FIGURE 2: Bilateral guarantee rate model.

requirements, both $W_{99\%}$ and $W_{1\%}$ need to be calculated, and then select the one with the larger absolute value. That is,

$$\left|W_{\text{design}}\right| = \max\left\{\left|W_{0.99,\text{design}}\right|, \left|W_{0.01,\text{design}}\right|\right\}. \tag{4}$$

The meanings of the above symbols are as follows:

W_{design}: design extreme wind load with at least 98% guarantee rate

$W_{0.99,\text{design}}$: design extreme wind load meeting 99% guarantee rate

$W_{0.01,\text{design}}$: design extreme wind load meeting 1% guarantee rate
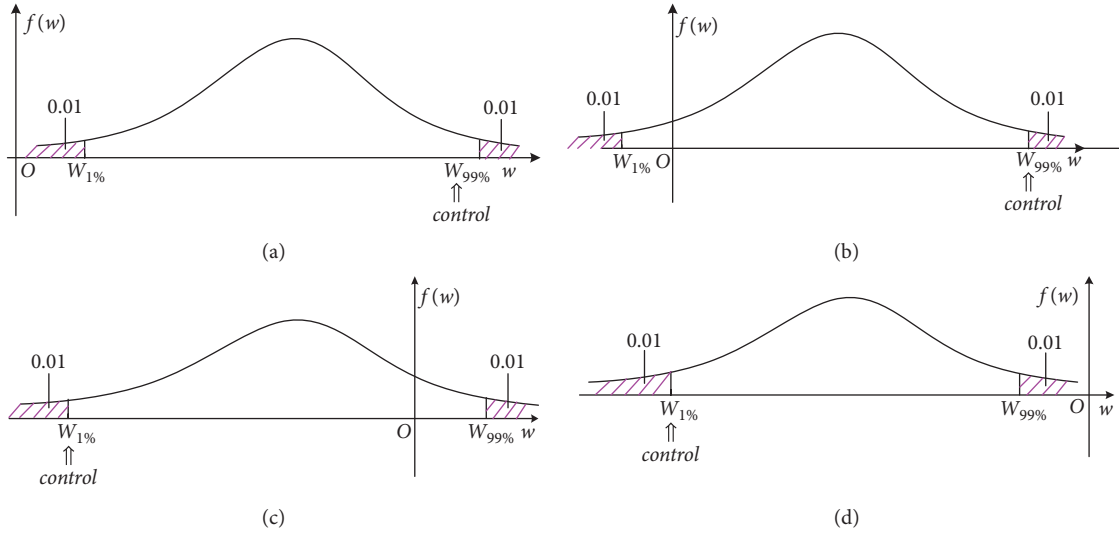
FIGURE 3: Diagram of relationship between quantile and guarantee rate. (a) Illustration of design extreme wind pressure controlled by $W_{99\%}$. (b) Illustration of design extreme wind pressure controlled by $W_{99\%}$. (c) Illustration of design extreme wind pressure controlled by $W_{1\%}$. (d) Illustration of design extreme wind pressure controlled by $W_{1\%}$.

TABLE 1: Quantile value in different cases.

Case number	Corresponding figure number	Wind load is positive or negative		Wind load controlling quantile value
		Quantile 99%	Quantile 1%	
1	Figure 3(a)	Positive	Positive	$W_{99\%}$
2	Figure 3(b)	Positive	Negative	$W_{99\%}$
3	Figure 3(c)	Positive	Negative	$W_{1\%}$
4	Figure 3(d)	Negative	Negative	$W_{1\%}$

For multiple extreme wind pressure probability distributions, at a certain measuring point under N wind angles, there are N extreme wind pressure coefficient time histories, from which N S-shaped probability distribution can be obtained. For these N wind pressure coefficient time histories, there is design wind load $\geq$ load effect. The design wind load W_{design} can be obtained by several probability distribution curves. In the following figures, for simplicity, two S-shaped probability distribution curves are used to illustrate the idea of solving the guarantee rate (in fact, there are N S-shaped probability distribution curves; the solving method is the same as that for two S-shaped curves), as shown in Figures 4(a) and 4(b). In these two figures, W_1 and W_2 are the wind pressure extremum corresponding to a certain probability on the probability distribution curve of wind pressure extremum.

Define $W_{0.99,design}$ as design wind load. Here, $|W_{0.99,design}| = \max\{|W_1|, |W_2|\}$; it can be seen from Figure 4(a) that when guarantee rate $P < 0.99$, wind load W (load effect) corresponding to red and blue curves is both less than or equal to W_2; here, W_2 is design wind load, and $W_2 = W_{0.99,design} = \max\{|W_i|, (i = 1, 2)\}$.

Define $W_{0.01,design}$ as design wind load. Here, $|W_{0.01,design}| = \max\{|W_1|, |W_2|\}$, and it can be seen from Figure 4(b) that when guarantee rate $P > 0.01$, wind load W (load effect) corresponding to red and blue curves is both less than or equal to W_1; here, W_1 is design wind load, and $W_1 = W_{0.01,design} = \max\{|W_i|, (i = 1, 2)\}$.

The above analysis shows that if wind load $W \leq |W_{design}|$, then

when $P = 0.99$, $W_{0.99,design}$ satisfies $|W_{0.99,design}| = \max\{|W_i|, (i = 1, 2, \ldots N)\}$ and

when $P = 0.01$, $W_{0.01,design}$ satisfies $|W_{0.01,design}| = \max\{|W_i|, (i = 1, 2, \ldots N)\}$.

Determine W_{design} and enable it satisfying $|W_{design}| = \max\{|W_{0.99,design}|, |W_{0.01,design}|\}$.

The symbols in the above formulas are defined the same as those in (4). The word "at least" in the above definition of W_{design} means that the area of non-shaded area in Figures 5(a) and 5(b) is greater than 98%. The design extreme wind loads correspond to the quantiles $W_{0.99,design}$ and $W_{0.01,design}$. Refer to Figures 5(a) and 5(b) below.

The range of guarantee rate values in Figures 5(a) and 5(b) is described in Tables 2 and 3:

Combining with (4), it can be inferred that the guarantee rate corresponding to W_{design} is more than 98%. As shown in Figures 5(a) and 5(b), because the distance $|\mu_W - W_{0.01,de\ sign}|$ between the left quantile and the mean μ_W is not necessarily equal to the distance $|W_{0.99,design} - \mu_W|$ between the right quantile and the mean μ_W, this method is called "asymmetric quantile truncation method" with 98%
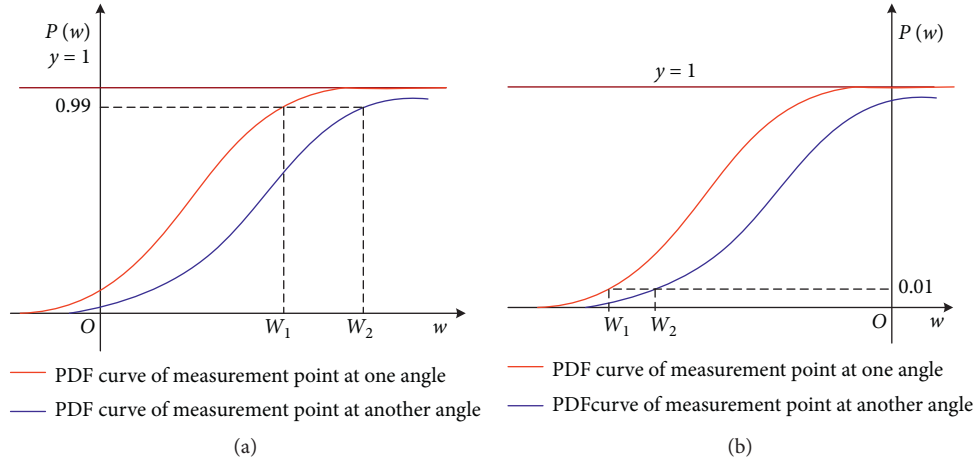
Figure 4: Diagram of probability distribution curve corresponding to guarantee rate. (a) Probability distribution curve with 99% assurance rate. (b) Probability distribution curve with 1% assurance rate.
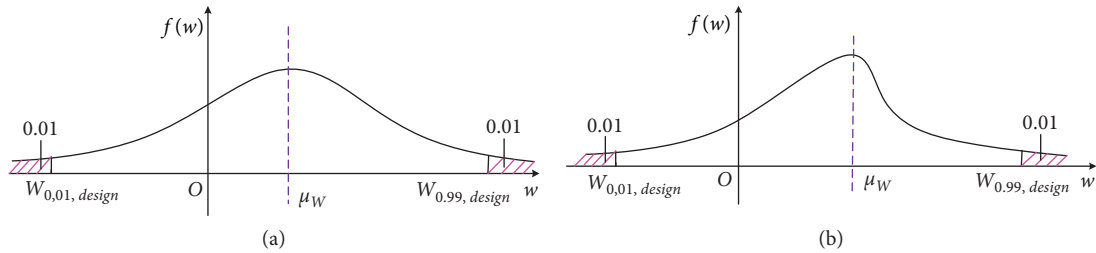

Figure 5: Diagram of the relationship between two design wind load: $W_{0.99,\text{design}}$ and $W_{0.01,\text{design}}$. (a) Gaussian distribution case; (b) non-Gaussian distribution case.

Table 2: Guarantee rate range (1).

Range of guarantee rate	Condition
>98%	When $W_{0.99,\text{design}}$ and $W_{0.01,\text{design}}$ are not symmetric with respect to μ_W
= 98%	When $W_{0.99,\text{design}}$ and $W_{0.01,\text{design}}$ are symmetric with respect to μ_W

Table 3: Guarantee rate range (2).

Range of guarantee rate	Condition
>98%	When $W_{0.01,\text{design}} + 2\left(\mu_W - W_{0.01,\text{design}}\right) > W_{0.99,\text{design}}$ When $W_{0.01,\text{design}} + 2\left(\mu_W - W_{0.01,\text{design}}\right) < W_{0.99,\text{design}}$
= 98%	When $W_{0.01,\text{design}} + 2\left(\mu_W - W_{0.01,\text{design}}\right) = W_{0.99,\text{design}}$

guarantee rate in this case. It is similar to other guarantee rate values.

3.3. Numerical Algorithm

3.3.1. Monte Carlo Sampling Simulation of Original Wind Speed Data.
In the process of extreme value theory modeling and parameter fitting, problems such as missing wind speed sample data and data singularity are often

encountered, which will decrease the accuracy of parameter fitting and the estimation of extreme wind speed, and Monte Carlo sampling of original data can solve these problems [29]. Based on the basic principle of Monte Carlo, the specific calculation steps of the Algorithm 1 are as follows:

3.3.2. Numerical Algorithm.
Based on model (8) and the above theoretical analysis of the guarantee rate, this paper proposes an algorithm to calculate design wind load

---

(1) The original wind speed sampling data is classified and counted according to the wind direction. There are 6000 wind speed samples at a certain wind direction in this numerical calculation case. The kernel density estimation method is used to fit these 6000 wind speed samples to obtain 6000 probability values $P_i = (i = 1, \ldots, 6000)$ corresponding to the probability distribution curve.

(2) The coordinates of 6000 points on the probability distribution curve are obtained : $(U_1, P_1), (U_2, P_2), \ldots, (U_{6000}, P_{6000})$.

(3) According to the fitting results calculated in Step 2, a mathematical model can be obtained: $P = F(x)$. Then, U is substituted as an independent variable.

(4) For $P = f(x)$ in Step 3, find its inverse function: $F^{-1}(x)$.

(5) Substitute N random numbers $P_1, P_2 \ldots, P_N$ generated by uniform distribution $U(0, 1)$ into $F^{-1}(P_i) = x_i$.

(6) In this way, the sample of Monte Carlo simulation with sample size of N is obtained: $x_1, x_2, \ldots, x_N$. These are the new extreme wind speed samples with sample size of N: $U_1, U_2, \ldots, U_N$.

ALGORITHM 1: Process of original wind speed data.

according to the wind speed data of wind tunnel test. The algorithm in this paper can be implemented by numerical calculation method, and the specific calculation process can be divided into the following steps:

Step 1: Determine nonlinear wind load probability model $\widehat{W} = 1/2\widehat{U}^2\widehat{C}_p$ (or $\widehat{W} = 1/2\widehat{U}^2\check{C}_p$), $\widehat{C}_p$ is maximum value, and $\check{C}_p$ is minimum value.

Step 2: Determine the time interval of two subsamples in the process of determining the probability model. This step is divided into the following two substeps:

(1) The time interval of extreme wind speed subsample is defined as: $T_{\widehat{U}}' = T_{\overline{U}}/m$. The length of duration of wind speed time history $\overline{U}$ is $T_{\overline{U}}$. The time history of the extreme wind speed $\widehat{U}$ (i.e., sub-sample) and its time interval $T_{\widehat{U}}'$ are determined.

(2) The time interval of extreme wind pressure coefficient is defined as $T_{C_p}' = T_{C_p}/n$. In this paper, the value can be calculated: $10 = 6000/600$. The time history of extreme wind pressure coefficient $\widehat{C}_p(\check{C}_p)$ determined by the wind pressure coefficient time history C_p is 600.

Step 3: Since $\widehat{U}$ and $\widehat{C}_p(\check{C}_p)$ are independent of each other, find the probability distribution that they obey.

Step 4: For a certain measuring point, find probability distribution $f_{\widehat{C}_p}(\theta_i, h), i = 1, 2, \ldots, N$ of $\widehat{C}_p(\theta_i, h)$. Follow the same step for $\check{C}_p(\theta_i, h)$.

Step 5: For a certain measuring point, calculate the converted wind speed $\widehat{U}_2$ according to height from the original extreme wind speed $\widehat{U}_1$, and then do the Monte Carlo sampling simulation to find the simulated extreme wind speed $\widehat{U}$ out of large sample, i.e., $\widehat{U}(\theta_i, h), i = 1, 2, \ldots, N$.

Step 6: For a certain measuring point, calculate the probability distribution $f_{\widehat{U}}(\theta_i, h), i = 1, 2, 3 \ldots N$ of $\widehat{U}(\theta_i, h)$, and the probability distribution $f_{\widehat{U}^2}(\theta_i, h), i = 1, 2, 3 \ldots N$ of $\widehat{U}^2(\theta_i, h)$.

Step 7: For a certain measuring point, find the probability distribution $f_{Z_1}(\theta_i, h), i = 1, 2, 3 \ldots N$ of $Z_1(\theta_i, h) = \widehat{U}^2 \cdot \widehat{C}_p$.

Step 8: For a certain measuring point, find the probability distribution $f_{Z_1}(\theta_i, h), i = 1, 2 \ldots N$ of $Z_1(\theta_i, h) = 1/2\rho\widehat{U}^2 \cdot \widehat{C}_p$.

Step 9: For a certain measuring point, calculate the design wind load $W_{j,\text{design}}$, $(j = 1, 2, 3, \ldots, m)$ with identical guarantee rate, and m is the total number of measuring points.

For different measurement points, the same guarantee rate corresponds to different quantile values, so the algorithm is referred to as "based on identical guarantee rate." The maximum and minimum wind load sequences can be calculated as follows:

(1) Calculation of wind load maximum sequence: the wind load corresponding to 99% (or 99.9%) guarantee percentile of each distribution is maximum design wind load $\widehat{W}_{0.99}(\theta_I, h)$. The wind load value corresponding 1% (or 0.1%) guarantee rate quantile of each distribution is minimum design wind load $\widehat{W}_{0.01}(\theta_I, h)$ (negative maximum). If most of the maximum series samples are negative or all of them are negative, the design wind load can be calculated by $\widehat{W}_{0.01}(\theta_I, h)$. For example, the wind load time history is shown in Figure 6.

(2) Calculation of wind load minimum sequence: the wind load corresponding to 99% (or 99.9%) guarantee percentile of each distribution is maximum design wind load $\check{W}_{0.99}(\theta_I, h)$. If most of the samples of the minimum series are positive, or all are positive, the design wind load can be calculated by $\check{W}_{0.99}(\theta_I, h)$. For example, the wind load time history is shown in Figure 7.

The minimum design wind load W is taken as the value corresponding to the 1% (or 0.1%) guarantee rate quantile of each distribution $\check{W}_{0.99}(\theta_I, h)$ (negative maximum). Then, the maximum or minimum wind load mentioned above has
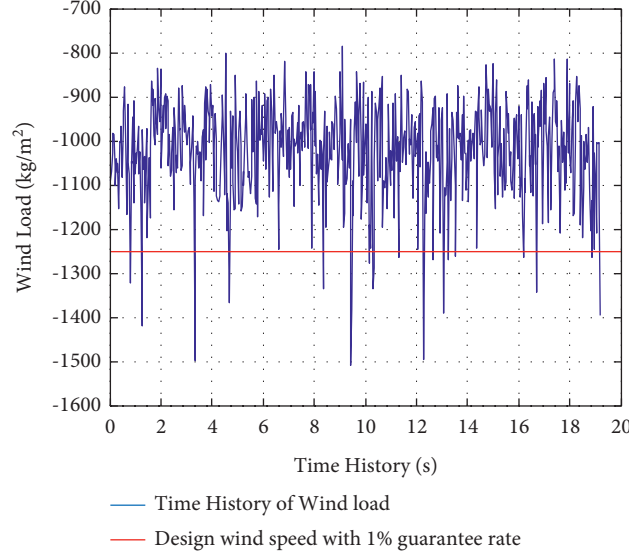
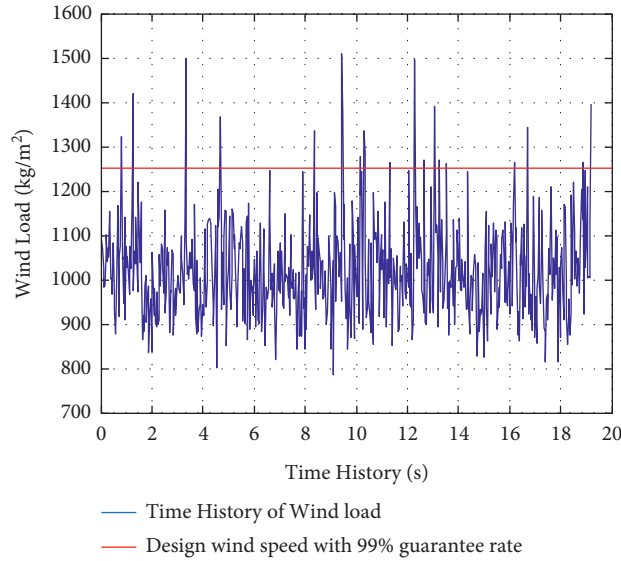FIGURE 6: Most of time history are negative, or all of them are negative.

FIGURE 7: Most of time history are positive, or all of them are positive.

$$
\begin{aligned}
&\widehat{W}_{0.99}\left(\theta_I, h\right)\text{satisfying}: \left|\widehat{W}_{0.99}\left(\theta_I, h\right)\right| = \max\left\{\left|\widehat{W}_{0.99}\left(\theta_I, h\right)\right|, I = 1, \ldots N\right\}, I \in [1, N], \\
&\widehat{W}_{0.01}\left(\theta_I, h\right) \text{satisfying}: \left|\widehat{W}_{0.01}\left(\theta_I, h\right)\right| = \max\left\{\left|\widehat{W}_{0.01}\left(\theta_i, h\right)\right|, i = 1, \ldots N\right\}, I \in [1, N], \\
&\widecheck{W}_{0.99}\left(\theta_I, h\right)\text{satisfying}: \left|\widecheck{W}_{0.99}\left(\theta_I, h\right)\right| = \max\left\{\left|\widecheck{W}_{0.99}\left(\theta_I, h\right)\right|, i = 1, \ldots N\right\}, I \in [1, N], \\
&\widecheck{W}_{0.01}\left(\theta_I, h\right)\text{satisfying}: \left|\widecheck{W}_{0.01}\left(\theta_I, h\right)\right| = \max\left\{\left|\widecheck{W}_{0.01}\left(\theta_I, h\right)\right|, i = 1, \ldots N\right\}, I \in [1, N].
\end{aligned}
\tag{5}
$$

According to the wind load maximum sequence and minimum sequence, design wind load of a measuring point is

$$
W_{j,\text{design}} = \max\left\{\left|\widehat{W}_{0.99}\left(\theta_I, h\right)\right|, \left|\widehat{W}_{0.01}\left(\theta_I, h\right)\right|, \left|\widecheck{W}_{0.99}\left(\theta_I, h\right)\right|, \left|\widecheck{W}_{0.01}\left(\theta_I, h\right)\right|\right\},
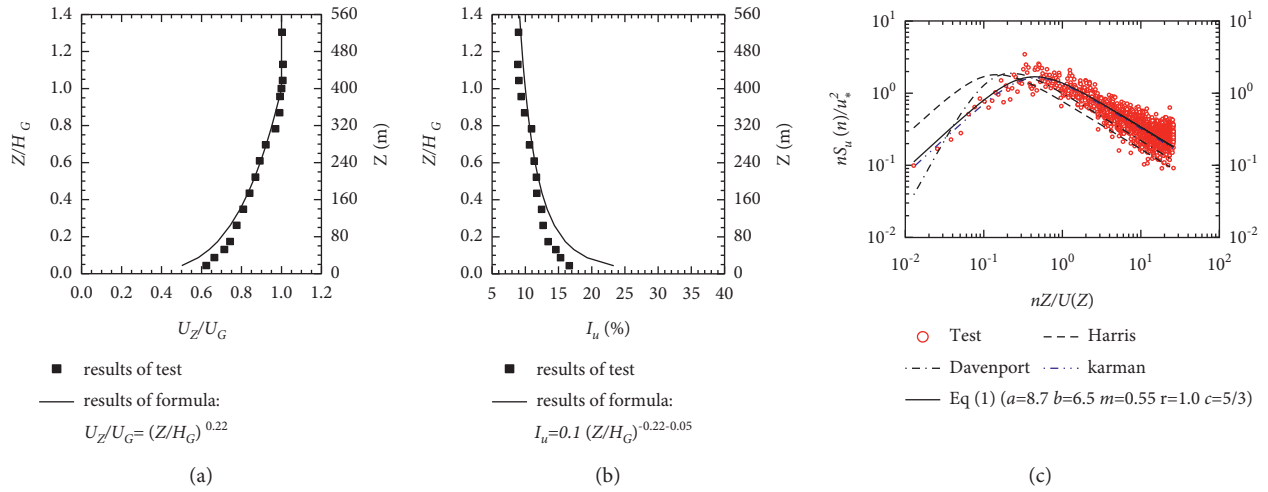\tag{6}
$$

FIGURE 8: Experimental wind field characteristics. (a) Mean wind speed profile. (b) Turbulence profile of along-wind. (c) Fluctuating wind spectrum of along-wind.
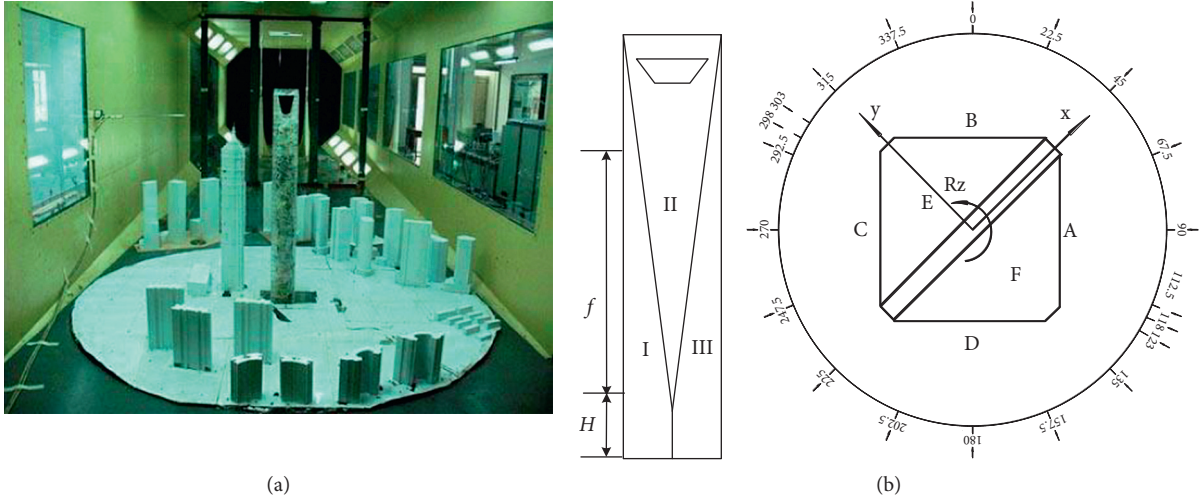

FIGURE 9: Setup, facade, wind direction, and coordinate axis of the rigid model. (a) Model test of rigid body pressure measurement. (b) Definition of model orientation, elevation, wind direction, and coordinate axis.

where $j = 1, 2 \ldots m$, $I \in [1, N]$, m is the total number of measuring points, N is the number of wind directions, and it is a positive integer.

For each measuring point, $4N$ wind load values were calculated by the above method based on $\widehat{U}$ and $\widehat{C}_p$ ($\check{C}_p$) at N wind directions. The maximum absolute value of these $4N$ values is the design extreme wind load of this measuring point. The design extreme wind load of 360° in any direction can be obtained by harmonic function fitting. If the layers in height direction and N wind directions in horizontal direction are considered at the same time, this wind load calculation method can be applied to each small block (each measuring point).

With the above method, the overall distribution of the maximum wind pressure of the equal probability design of the exterior envelope of the whole building can be obtained.

4. Research Methods Based on Wind Tunnel Test

4.1. Wind Field Simulation.
This study takes the Shanghai World Financial Center as an engineering background, and the pressure tests were carried out on a rigid model in the TJ-2 Wind Tunnel at Tongji University. The TJ-2 Wind Tunnel is a boundary layer tunnel of closed-circuit-type, and the working section of the tunnel is 3 m wide, 2.5 m high, and 15 m long. The achievable mean wind speed ranges from 0.5 m/s to 68.0 m/s, adjusted continuously. The mean wind speed profile together with the turbulence intensity for terrain category C was simulated mainly by using hybrid passive devices including roughness blocks, spirelets, and vertical-bar fences. The simulation result and the theoretical formula according to the Load code for the design of building structures by Ministry of Construction of the
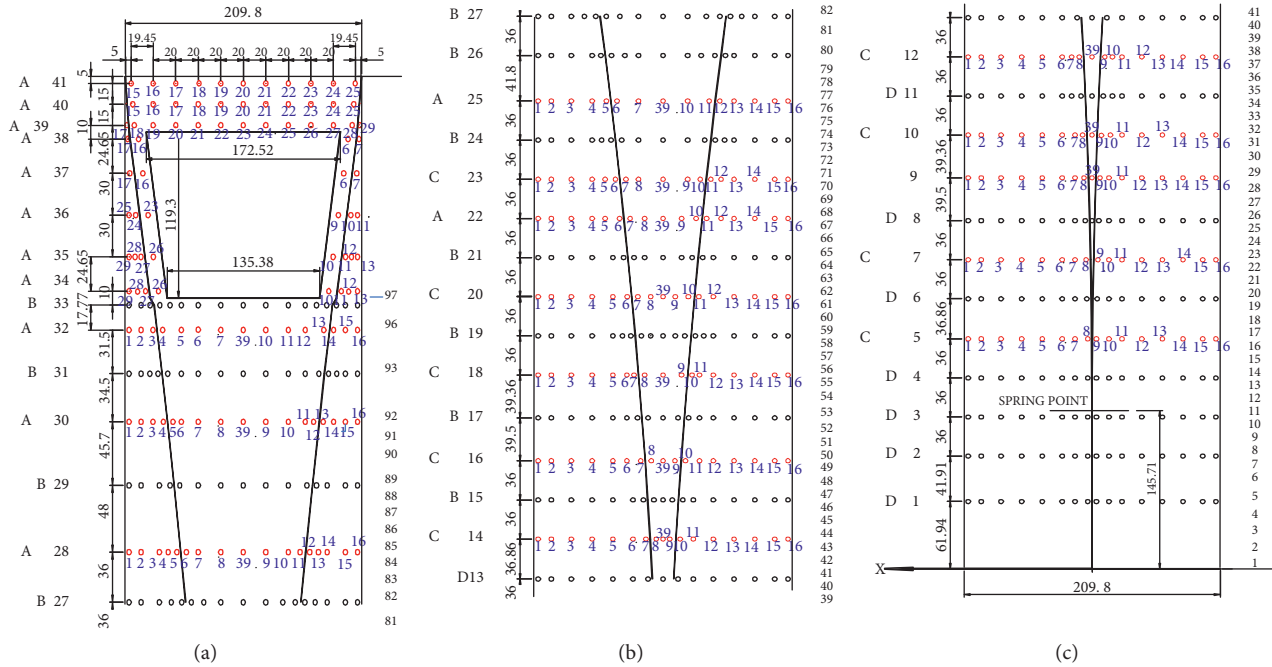
FIGURE 10: Layout of pressure measuring points on the front elevation of experimental measuring points (only A and C groups).

People's Republic of China (GB50009 - 2001) are shown in Figure 8.

4.2. Test Model.

The rigid model for wind tunnel pressure test is shown in Figure 9, together with the definitions of model orientation, wind direction angle, and coordinate axis of this rigid model. Each pressure signal was sampled with 6000 data points with a frequency of 312.5 Hz, which means that the sampling time is 19.2 s. Because of the limitations of the channels of the electronic scan valve, the signals of measuring taps could not be collected simultaneously at a time and should be divided into 4 groups of A, B, C, and D. The way of grouping situation, the characteristic size of model section, and the layout of surface pressure measurement taps are shown in Figure 7. It can be seen that pressure measurement taps were distributed on 22 levels, which were numbered from bottom to top of the model. There are 28 to 40 measurement taps in each level, changing with height. In this study, "L-i" is used to indicate the measurement taps, where L represents the number of levels, and i represents the measurement point number at this level. For example, "5–17" represents the 17 measurement points of the 5th level.

4.3. Test Conditions.

Corresponding to the 1:350 length scales, the total height of this model is 1.4 m. In this test, the reference wind speed was 14 m/s, which was monitored by a Pitot tube at 1.2 m height in wind tunnel (above the gradient height, equivalent to the actual 420 m height), about 1.0 m away from the side wall of the wind tunnel. Considering a recurrence period of 50 years, the actual wind speed corresponding to the reference point is 52.93 m/s according to the conversion of basic wind pressure of the C-type

landform in Shanghai, and then the wind velocity ratio can be deduced to be $\lambda_V = 0.2645$. The time ratio is $\lambda_t = \lambda_L / \lambda_V = 0.0108$, which can be deduced by the dimensional analysis method.

5. Numerical Results and Analysis

5.1. Analysis of Calculated Wind Load.

In an appearance in Figure 10 the Shanghai world financial center is a 57 m × 57 m × 492 m square cylinder, and there is a diagonal line from northeast to southwest at the top. Take one point at each of the two vertical edges from northwest to southeast 52 meters above the ground and cut an oblique section through the diagonal line and the two points, forming the shape of Shanghai World Financial Center. Here, the front elevation in Figure 11 is divided into left elevation I, middle-inclined section 2, and right elevation III. Figure 9(b) is the schematic diagram of front elevation zoning.

Through the wind tunnel test described in Section 4, the test data are obtained. According to the test data, the numerical method is applied to calculate the wind load with an identical guarantee rate. Based on the wind tunnel experiment described in Section 4.1, the wind speed sample data of each layer are obtained by sampling the wind speed in the wind tunnel. According to these data, the numerical calculation is carried out according to the algorithm implementation steps in Section 3.3, and the wind load and wind pressure are analyzed according to the intermediate and final results of the calculation process. Due to the complex building shape and too many measuring points in this example, in order to grasp the core idea and highlight the trend law, the measuring points on the seventh floor are selected to analyze the calculation results of wind load. The arrangement of measuring points and the relationship
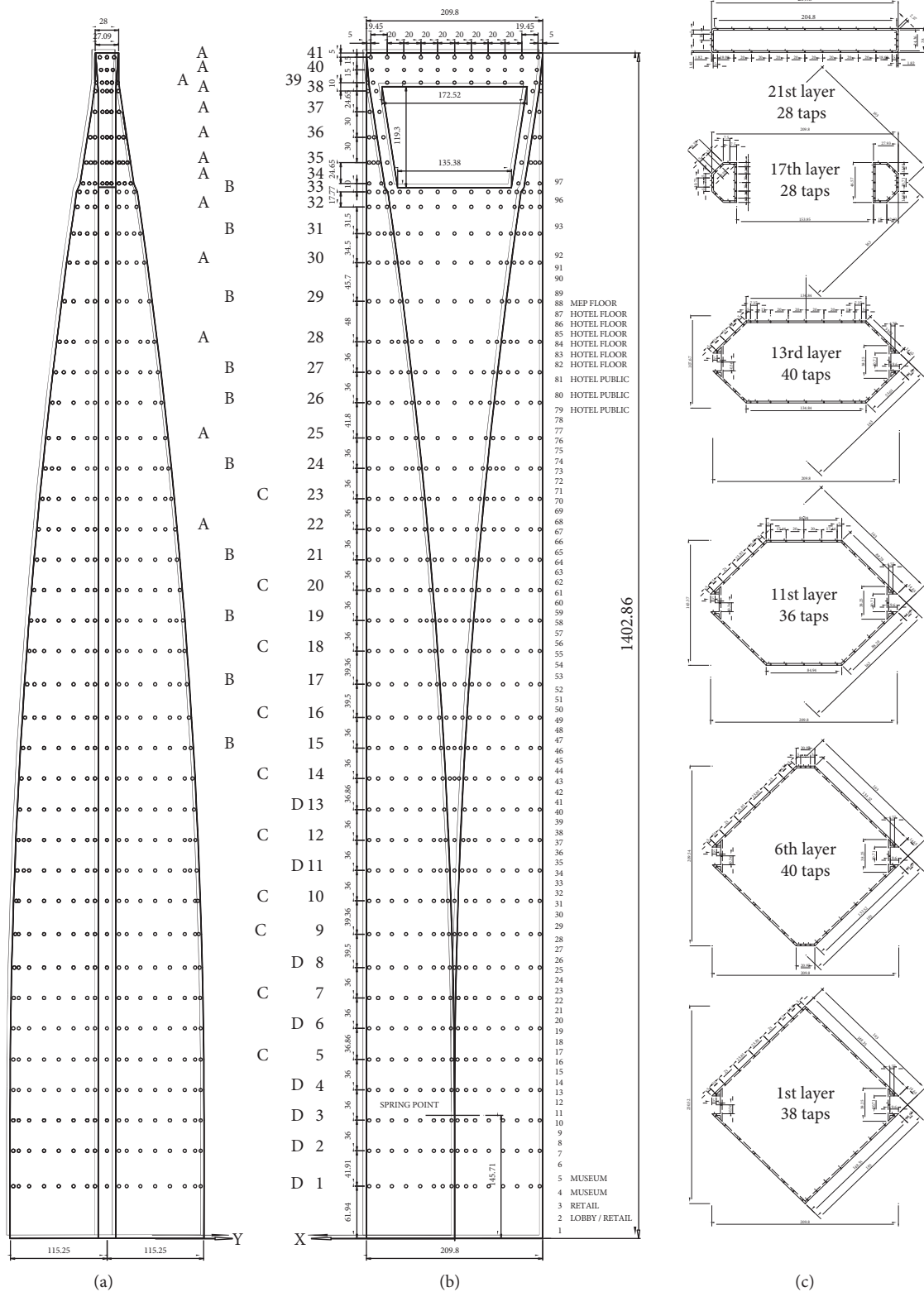
FIGURE 11: Layout of measuring points for pressure measurement model of Shanghai World Financial Center. (a) Side elevation. (b) Front elevation. (c) Cross section on typical height.

between wind direction and angle on the seventh floor are shown in Figure 12, and the calculation results are listed in Table 4.

According to Figure 10(b), the wind load values of the measuring points deployed at 16th, 18th, and 20th floors are negative, and they are shown in Table 5. The results show
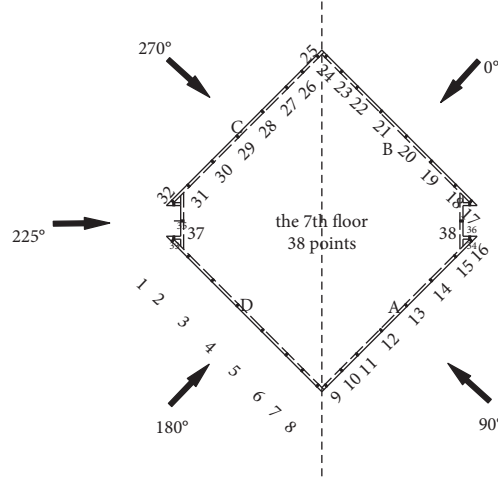
Figure 12: Cross section of the 7th measurement level and definition of wind direction angle.

that the direction of wind load is away from the building surface, which is suction.

According to Figures 9(b) and 10(b), the wind load values of the measuring points deployed at the junction of the left elevation I and the middle-inclined section 2 of the front elevation are shown in Table 6. The results show that the wind loads change greatly at the junction of the two outer inclined planes I and II (see Table 6 and Figure 13(c)), which is mainly due to the influence of incoming flow separation, reattachment, and vortex shedding. In the junction area of two inclined planes, the wind pressure exhibits strong non-Gaussian property, and the wind pressure of the measuring point in the structure surface area with strong non-Gaussian property is more sensitive to the change of wind direction angle and the surface structure of the building object.

The wind load of the measuring point at the edge of the building opening is relatively small (see Table 7 and Figure 1(d)), and the wind load value at the edge of the high-rise opening is close to or even smaller than that of the lower floor in the same column. It is because the building opening can effectively reduce the wind pressure coefficient.

The above analysis shows that the wind load calculated by this algorithm is consistent with the actual situation.

5.2. Fitting of Probability Distribution Function

5.2.1. Minimal Polynomial Fitting. In this paper, the polynomial fitting method and kernel density estimation method are used to find the probability distribution function of discrete wind speed sample data. In this section, the two algorithms and parameter selection are briefly introduced. Polynomial fitting is to use a polynomial expansion to fit all the observation points in a small analysis area, which contains several points in analysis grid to obtain the objective analysis field of the observation data. The expansion coefficient is determined by least-square fitting. In the numerical experiment of polynomial fitting, it is found that the fitting results do not change with increasing of the order of polynomial, and the fitting result is better when the order of

the polynomial is 20. When the order is more or less than 20, the fitting curve begins to oscillate up and down.

5.2.2. Kernel Density Estimation Fitting. Kernel density estimation is a density estimation method proposed in the 1950s and 1960s. It is an effective nonparametric estimation method. Supposing that $x^1, x^2, \ldots, x^N$ are samples of random variable x, and the probability density function of variable x is $f(x)$, then the kernel density estimation of f can be expressed as

$$\widehat{f}(x) = \frac{1}{Nh} \sum_{i=1}^{N} K\left(\frac{x - x^i}{h}\right), \tag{7}$$

where h is the bandwidth, N is the sample function, $K(\cdot)$ is the kernel function, the selection principle of $K(\cdot)$ is Borel measurable in its measure space, and it has the following asymptotically unbiased properties:

$$\int K(u)\mathrm{d}u = 1,$$

$$\int uK(u)\mathrm{d}u = 0, \tag{8}$$

$$\int u^2 K(u)\mathrm{d}u = \mu_2(K) > 0.$$

It can be proved by (8) that when the number of samples $n \longrightarrow \infty$, the window width $h \longrightarrow 0$ and $nh \longrightarrow 0$, $\widehat{f}(v)$ converges to $f(v)$ in probability. Therefore, when the sample data is known, the accuracy of $\widehat{f}(v)$ depends entirely on the choice of kernel function $K(\cdot)$ and window width h. When the window width h is fixed, different kernel functions have different effects on $\widehat{f}(v)$. The influence of the two is equivalent. The commonly used kernel functions are Uniform, Triangle, Epanechnikov, and Gaussian. Different kernel functions have different contributions to each sample point to be estimated according to the distance. The choice of kernel function is usually not the key of density estimation, and the bandwidth has a great influence on the smoothness of the model. If the bandwidth is very large, more points will

TABLE 4: Statistical value of wind load on different floors.

Measuring point no.	7-1	7-2	7-3	7-4	7-5	7-6	7-7	7-8	7-9	7-10	7-11	7-12	7-13	7-14	7-15	7-16	7-17	7-18	7-19
Wind load	-0.612	-0.769	-0.357	-0.382	-0.445	-0.468	-0.47	-0.563	-0.482	-0.508	-0.444	-0.417	-0.517	-0.593	-0.686	-0.594	-0.53	-0.394	-0.355
Measuring point no.	**7-20**	**7-21**	**7-22**	**7-23**	**7-24**	**7-25**	**7-26**	**7-27**	**7-28**	**7-29**	**7-30**	**7-31**	**7-32**	**7-33**	**7-34**	**7-35**	**7-36**	**7-37**	**7-38**
Wind load	-0.381	-0.487	-0.479	-0.488	0.88	1.029	0.957	0.938	0.946	0.95	0.96	0.965	0.895	2.097	0.994	1.162	1.008	1.268	1.13

TABLE 5: Wind loads at 16th, 18th and 20th floors.

Measuring point no.	Wind load	Measuring point no.	Wind load	Measuring point no.	Wind load	Measuring point no.	Wind load	Measuring point no.	Wind load	Measuring point no.	Wind load	Measuring point no.	Wind load	Measuring point no.	Wind load
20-1	-1.253	**20-2**	-1.206	**20-3**	-1.121	**20-4**	-0.897	**20-13**	-0.827	**20-14**	-0.967	**20-15**	-1.114	**20-16**	-1.122
18-1	-1.25	**18-2**	-1.175	**18-3**	-1.044	**18-4**	-0.878	**18-13**	-0.773	**18-14**	-0.916	**18-15**	-1.016	**18-16**	-1.102
16-1	-0.96	**16-2**	-1.077	**16-3**	-0.936	**16-4**	-0.792	**16-13**	-0.727	**16-14**	-0.844	**16-15**	-0.952	**16-16**	-0.497

TABLE 6: Wind loads at junction of plane I and II.

Measuring point no.	28-5	28-6	25-5	25-6	23-6	23-7	22-6	22-7	20-6	20-7	18-7	18-8	16-7	16-8
Wind load	1.044	−1.412	0.959	−1.318	0.921	−1.091	0.877	−1.013	0.819	−0.949	0.787	−0.787	0.706	−0.701

(a)

(b)

(c)

(d)

(e)

(f)
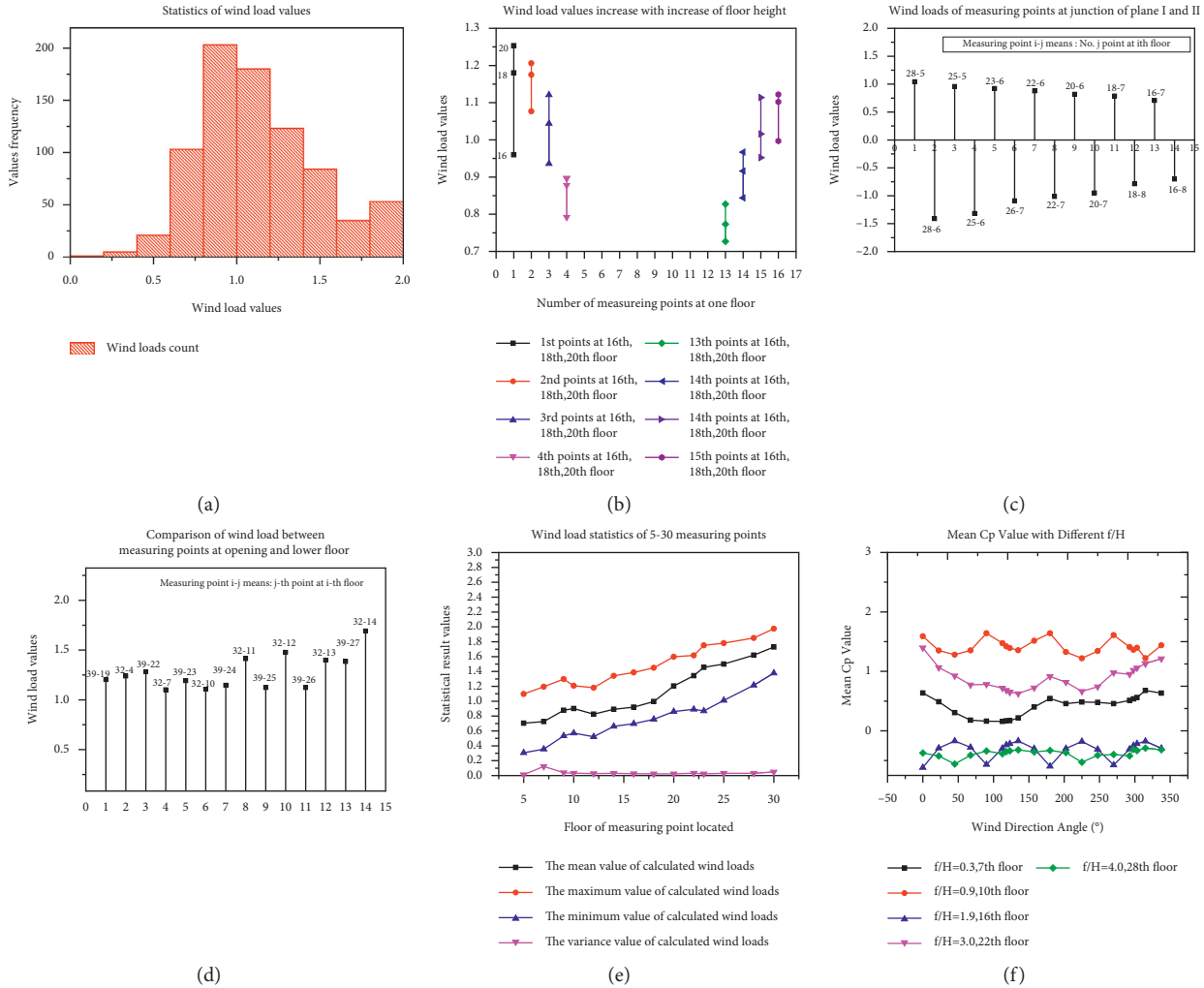
FIGURE 13: Wind load calculation results analysis.

have an impact on the density at x, and the farther points will weaken the weight of the closer points, the deviation of kernel estimation is large, and the variance is small, so the peak values of the main part is covered, and the curve is too smooth. On the contrary, if the bandwidth is too small, the weight of each point has a large drop due to the influence of distance, and the deviation of kernel estimation is small, the variance is large, and the curve presents the characteristics of multipeak instability. In this paper, Gaussian function is chosen as the kernel function.

5.3. Analysis of Wind Pressure Distribution. The wind pressure coefficient can be calculated according to the experimental wind pressure sample data. Figure 14 shows the average wind pressure coefficient on the surface of the

experimental model when the incoming wind direction angle is several typical angles. The mean (cpmean), root mean square (cprms), skewness (cpsk), and kurtosis (cpku) are calculated. In this paper, the wind direction angle 180° is taken as an example. At 180° wind direction angle, the opposite left elevation I is equivalent to that at the wind direction angle of 135°, the inclined section 2 is equivalent to that at the wind direction angle of 180°, and the right elevation III is equivalent to that at the wind direction angle of 225° (135°).

It can be seen from Figure 15 that the wind pressure coefficients range from −1 to −0.2 on the left side elevation I. The wind pressure coefficients on the 135° leeward side are negative. The wind pressure coefficients at inclined section 2 range from −1 to −0.7, which is equivalent to a 180° wind angle on the leeward side of the wake area and bears the

TABLE 7: Wind load of measuring points near opening.

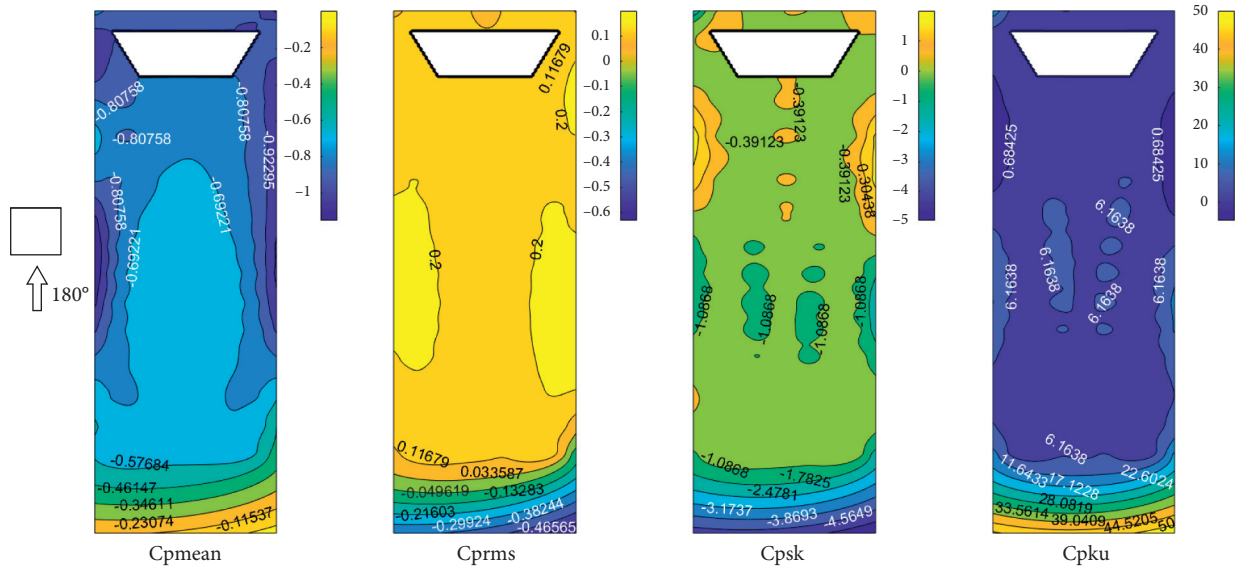| Measuring point no.	39-19	39-20	39-21	39-22	39-23	39-24	39-25	39-26	39-27	32-4	32-5	32-6	32-7	32-10	32-11	32-12	32-13	32-14
Wind load	−1.345	−1.216	−1.204	−1.283	−1.192	−1.147	−1.123	−1.123	−1.385	−1.239	−1.149	−1.139	−1.102	−1.106	−1.414	−1.478	−1.398	−1.691
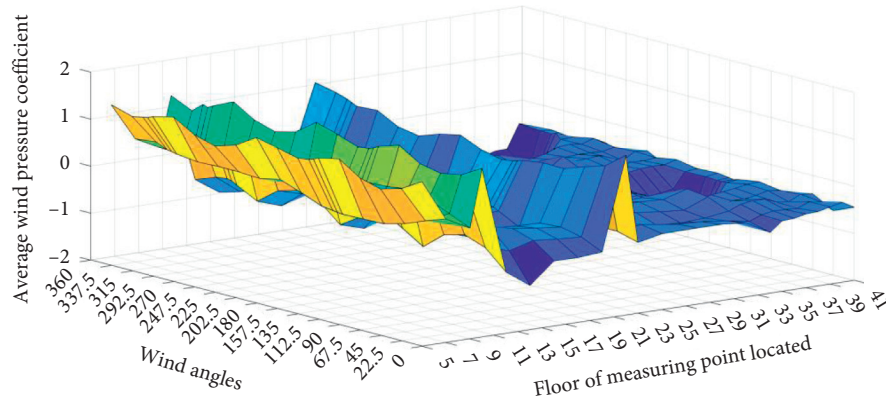
Figure 14: Mean wind pressure coefficient.

Figure 15: Distribution of statistics of building facade wind pressure coefficient at 180° wind direction.

suction. On the leeward side, the middle and lower parts bear the least suction, and the suction gradually increases spreading around. The deviation at left elevation I ranges from −5 to −1−1. Skewness at inclined section 2 ranges from −2 to −1. The deviations at the right elevation range from −5 to −1. The kurtosis at the left elevation ranges from 0 to 40. The kurtosis at inclined section 2 ranges from 0 to 7. The kurtosis of the right elevation III ranges from 0 to 50.

From the experimental data and results, it is known that wind loads at the oblique section 2 follow non-Gaussian distribution. The left elevation I and the right elevation III belong to a strong non-Gaussian distribution area. The vortex movement such as the separation and reattachment of the incoming flow on the building surface changes the disorganization and uniformity of the turbulence movement in the original wind field, resulting in a non-Gaussian wind field. The wind pressure on the envelope surface is very sensitive to the change of the incoming flow turbulence intensity, and the non-Gaussian characteristics increase with the increase of the turbulence intensity. The results show that

the variation of wind pressure with wind direction angle is more sensitive in the region with strong non-Gaussian characteristics.

5.4. Probability Distribution of Fluctuating Wind Pressure. The tail of wind pressure probability distribution directly determines the calculation result of wind pressure extreme value, so the fitting of tail region in probability fitting diagram is the focus of attention. In order to check the fitting of the tail of wind pressure probability distribution more accurately, the longitudinal probability density is set as logarithmic coordinate system, and the time history of wind pressure coefficient on building surface is fitted by normal distribution, Gamma distribution, and Weibull distribution function respectively. Figure 16 shows the detailed fitting of wind pressure probability distribution. Figures 16(a) and 16(f) show that, in the region of positive wind pressure, fluctuating wind pressure is in good agreement with Gaussian distribution, and its probability distribution can be
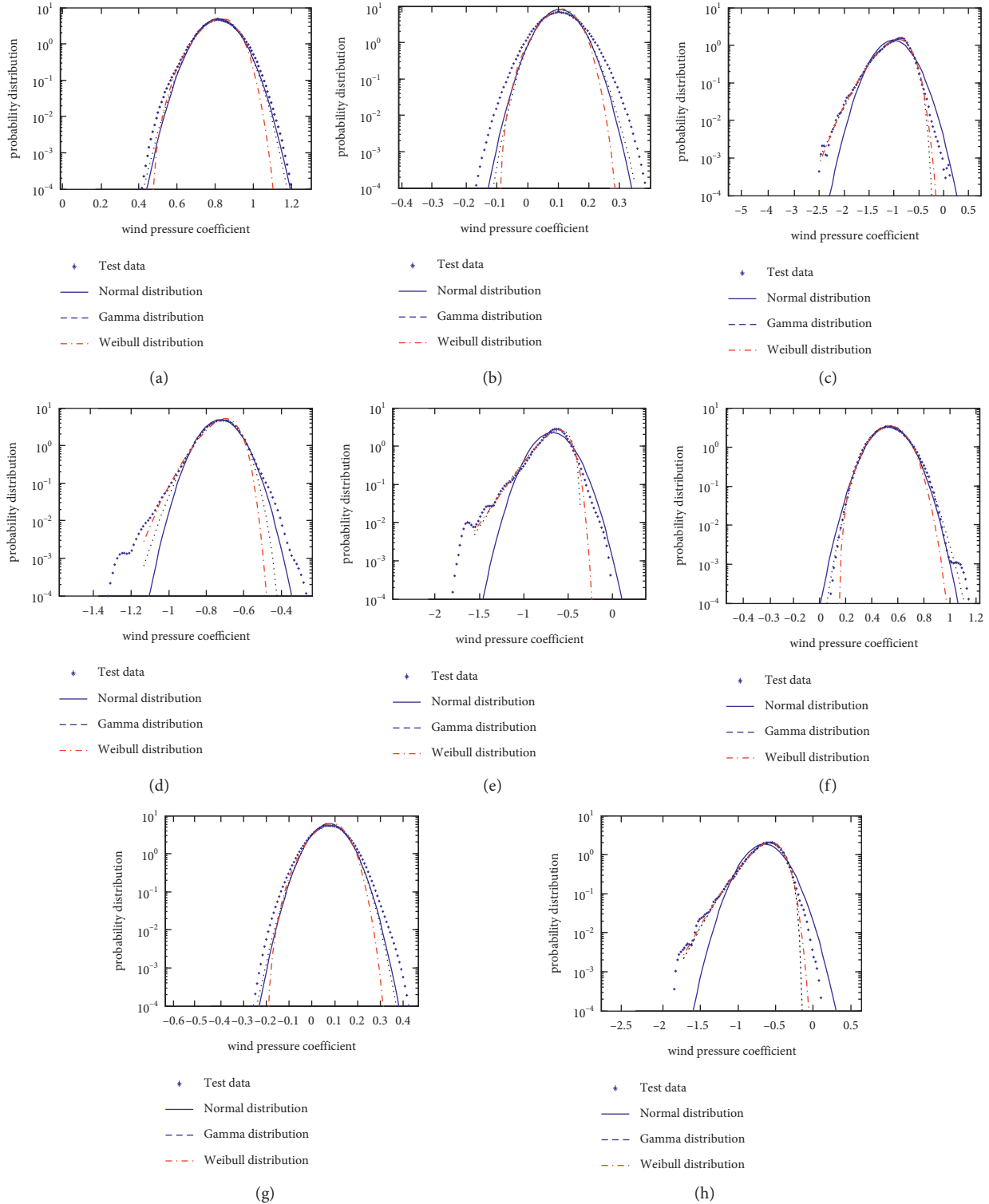
FIGURE 16: Probability density fitting diagram of wind pressure coefficient at typical measurement points. (a) 0° measurement point 28–39. (b) 45° measurement point 28–39. (c) 90° measurement point 28–39. (d) 135° measurement point 28–39. (e) 180° measurement point 28–39. (f) 45° measurement point 5-3. (g) 90° measurement point 5-3. (h) 135° measurement point 5-3.

well described by normal distribution and Gamma distribution, while Weibull distribution is relatively poor in describing these probability distributions (see Figures 16(a), 16(b), 16(f), and 16(j)). Figures 16(c)–16(e) show that the

probability distribution of wind pressure time history at each measuring point in the separation zone of incoming flow on the roof is obviously non-Gaussian and has obvious negative skewness. As for the characteristics of spatial flow field, due

(a)

(b)

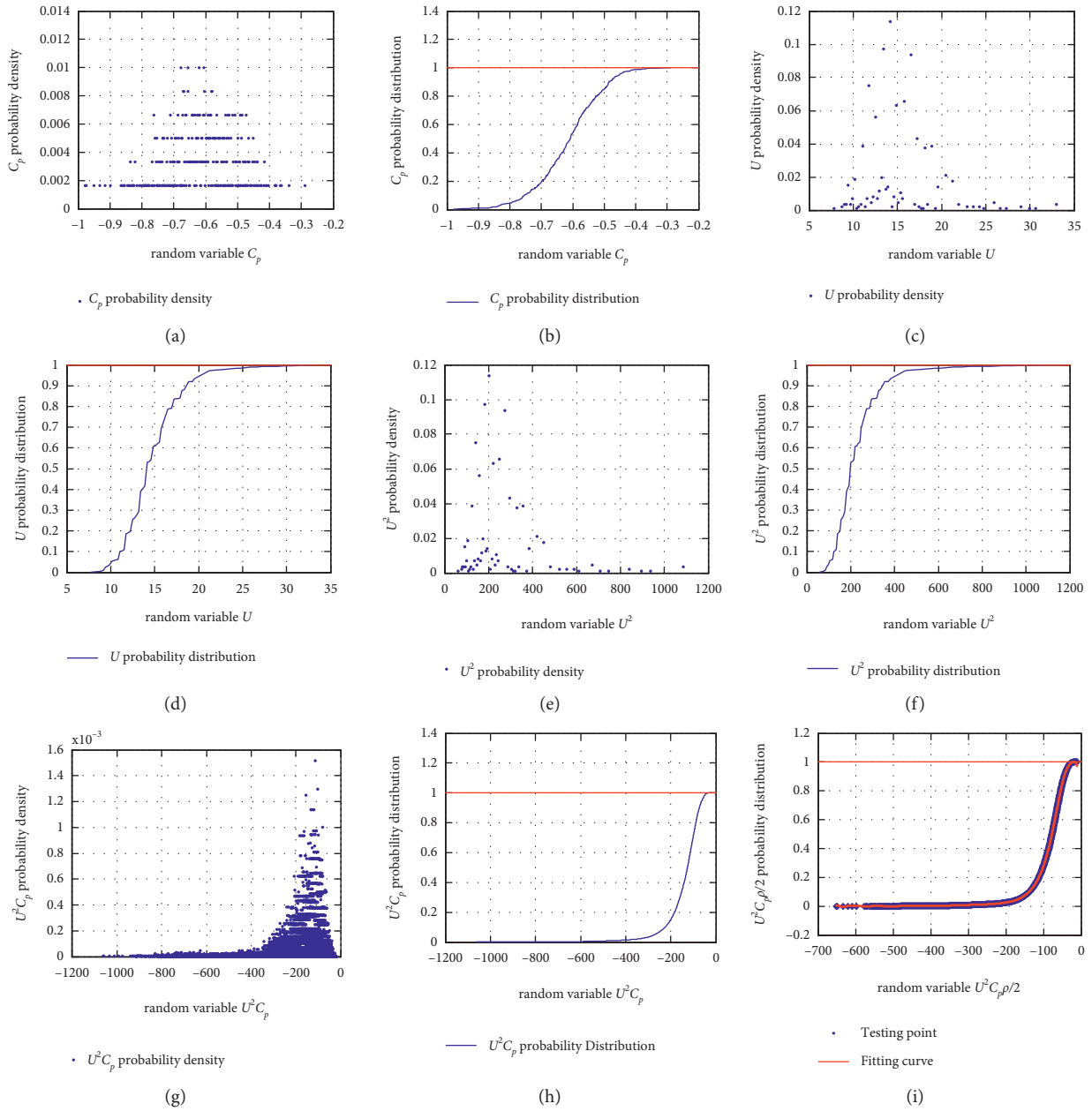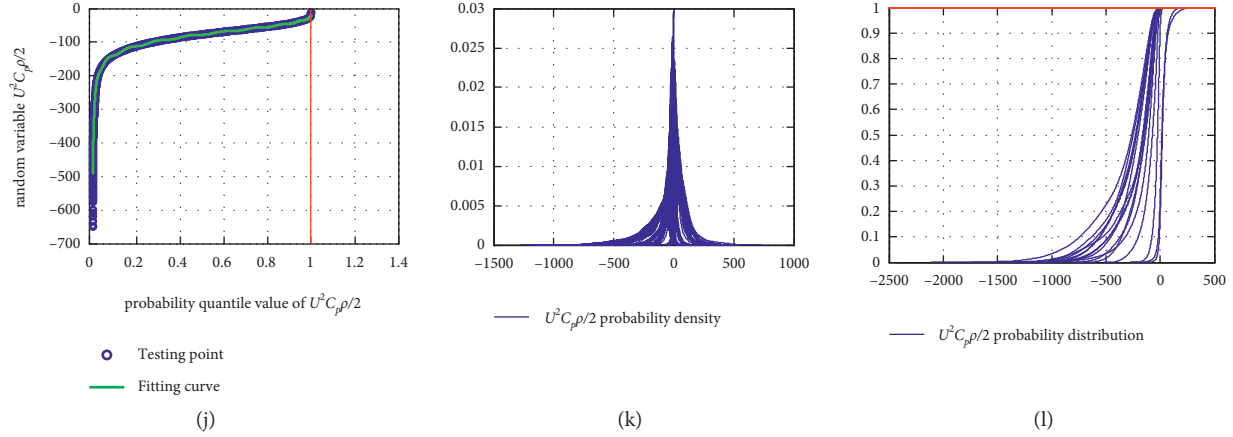(c)

(d)

(e)

(f)

(g)

(h)

(i)

Figure 17: Continued.

FIGURE 17: The probability density and probability distribution diagram of random variables in the intermediate process of the algorithm. (a) Probability density diagram of wind pressure coefficient C_p time history of measuring point 41-1 at 0° wind direction. (b) Probability distribution diagram of wind pressure coefficient C_p time history of measuring point 41-1 at 0° wind direction. (c) Probability density diagram of wind pressure coefficient U time history of measuring point 41-1. (d) Probability distribution diagram of wind pressure coefficient U time history of measuring point 41-1 at 0° wind direction. (e) Probability density diagram of U^2 time history of measuring point 41-1 at 0° wind direction. (f) Probability distribution diagram of U^2 time history of measuring point 41-1 at 0° wind direction. (g) Probability density diagram of $U^2 C_p$ time history of measuring point 41-1 at 0° wind direction. (h) Probability distribution diagram of $U^2 C_p$ time history of measuring point 41-1 at 0° wind direction. (i) 20-order polynomial fitting diagram of probability distribution of time history of measuring point 41-1 at 0° wind direction. (j) 20-order polynomial fitting diagram of inverse function of probability distribution of time history of measuring point 41-1 at 0° wind direction. (k) Diagram of superimposed probability density curves of points in top 4 of maximum wind pressure coefficient series (64 curves). (l) Diagram of superimposed probability distribution curves of points in top 4 of maximum wind pressure coefficient series (64 curves).

to the influence of airflow separation, vortex shedding, and the formation of characteristic turbulence, the correlation between the measuring points in the crosswind area parallel to the incoming flow is strong. On the windward side, the correlation between the measuring points decays rapidly, and the location between the measuring points is weak.

5.5. Probability Distribution Fitting in the Process of Calculation. In the process of numerical calculation, polynomial fitting and kernel density estimation are used to fit the discrete samples to obtain the probability distribution function of wind pressure extreme value, and the curve consistent with the expectation is obtained. The calculation example used in this paper includes 808 measuring points, for which experiments are carried out at 16 wind directions, and includes two cases of maximum sequence and minimum sequence in the process of calculation. Therefore, a total of $808 \times 16 \times 12 \times 2 = 310272$ figures of calculation results can be obtained in the calculation process. This paper takes measuring point 41-1 as an example. The method of calculating the wind load with identical guarantee rate at 0° (due north wind) extreme wind pressure coefficient at measuring point 41-1 obtains the relevant probability density and probability distribution graph. This paper lists 12 graphs of calculating the maximum wind load at 0° at measuring point 41-1 to illustrate the calculation results. As shown in Figures 17(b), 17(d), and 17(f), the fitting probability distribution curve of discrete points is smooth, and the value of probability gradually approaches 1, which is consistent with the distribution of wind load. The

polynomial curves of order 20 in Figures 17(i) and 17(j) are completely fitted with the test points, which ensures the accuracy of the algorithm.

6. Conclusion

Based on the basic theory of probability theory and the systematic analysis of the surrounding environment and turbulence of buildings, a random variable model is established to calculate the wind load. Based on this model, a numerical method is proposed. The algorithm is verified by the wind tunnel test data, and the following conclusions are obtained:

(1) It is not safe to use peak factor method to calculate extreme wind load of enclosure components in these areas. The investigation of wind disaster shows that it is the local damage caused by the separation of air flow and vortex shedding that leads to the larger damage of the envelope. Based on this, this paper studies the non-Gaussian characteristics of local wind pressure and its extreme value in high-rise buildings, so as to determine the extreme wind load reasonably and accurately.

(2) In this paper, the wind direction effect is considered in calculation method of the extreme wind load with the equivalent guarantee rate. For the windward side, because the wind pressure is close to Gaussian distribution, the extreme wind load based on identical guarantee rate is close to that based on traditional peak factor method. On the crosswind side,

because the wind pressure deviates from the Gaussian distribution, the extreme wind load with the identical guarantee rate is generally significantly larger than that based on the traditional peak factor method. On the leeward side, the results are between the windward side and the crosswind side.

(3) In the traditional method of calculating wind load, the "50-year return period" extreme value of the annual extreme value of wind speed at all wind direction and the wind pressure coefficient extreme value calculated by the peak factor method are used. Through the analysis of the test results, the proposed algorithm can reflect the situation of wind field, and its main advantages are accuracy and practicability. This method makes full use of the overall information of wind speed and wind pressure coefficient, so it is a reasonable numerical calculation method.

Data Availability

The data of pressure tests on a rigid model of Shanghai World Financial Center and data generated during research used to support the findings of this study were supplied by State Key Laboratory of Disaster Reduction in Civil Engineering at Tongji University in China under license and so cannot be made freely available. Requests for access to these data should be made to Tao Ye (yetao1982827@163.com).

Disclosure

Any opinions and concluding remarks presented here are entirely those of the authors.

Conflicts of Interest

The authors declare that there are no conflicts of interest regarding the publication of this paper.

Acknowledgments

References

[1] W. B. Li and S. N. Wang, "Design of wind resistance for lightweight steel building," in *Proceedings of the 2005 National Conference on Building Steel Structure Industry*, pp. 195–209, Beihai, Guangxi, China, April 2005.

[2] Y. F. Jing, Q. S. Yang, and Q. Li, "Typhoon damage investigation of claddings of light steel buildings," *Journal of Building Structures*, vol. suppl, no. 2, pp. 197–201, 2010.

[3] X. X. Zhang, "Estimation of Probabilistic Extreme Wind Load Effect with Consideration of Directionality and Uncertainty," Master Thesis, Texas Tech University, TX, USA, 2015.

[4] H. L. Xue, H. J. Liu, H. Y. Peng, Y. Luo, and K. Lin, "Wind load and structural parameters estimation from incomplete measurements," *Shock and Vibration*, vol. 2019, Article ID 4862983, 20 pages, 2019.

[5] A. G. Chowdhury, I. Canino, A. Mirmiran, N. Suksawang, and T. Baheru, "Wind-loading effects on roof-to-wall connections of timber residential buildings," *Journal of Engineering Mechanics*, vol. 139, no. 3, pp. 386–395, 2013.

[6] B. Yao, Y. Quan, and M. Gu, "Combination method of wind load about high-rise buildings based on probability analysis," *Journal of Tongji University*, vol. 44, pp. 1032–1037, 2016.

[7] X. Zhuang, X. Dong, J. M. Ding, and Y. M. Zhen, "Non-Gaussian features of wind pressure fluctuations on a rectangular high-rise building," *Journal of Building Structures*, vol. 37, pp. 13–18, 2016.

[8] F. Q. Meng, B. J. He, J. Zhu, D.-X. Zhao, A. Darko, and Z. Q. Zhao, "Sensitivity analysis of wind pressure coefficients on CAARC standard tall buildings in CFD simulations," *Journal of Building Engineering*, vol. 16, pp. 146–158, 2018.

[9] Y. Luo, "Extreme value theory and its application on wind load and response of structure," Ph D Thesis, Southwest Jiao tong University, Chengdu, China, 2018.

[10] B. Bhattacharyya and S. K. Dalui, "Investigation of mean wind pressures on 'E' plan shaped tall building," *Wind and Structures*, vol. 26, pp. 99–114, 2018.

[11] Y. Luo, G. Q. Huang, Q. S. H. Yang, and Y. J. Tian, "Calculation of peak non-Gaussian wind pressures based on high-order moments," *Journal of Building Structures*, vol. 39, no. 2, pp. 146–152, 2018.

[12] X. L. Ma, *Study on Non-gaussian Characteristic Analysis Methods of Wind Pressures on Building Surface*, Dalian University of Technology, Dalian, China, 2019.

[13] M. Mallick, A. Mohanta, A. Kumar, and V. Raj, "Modelling of wind pressure coefficients on C-shaped building models," *Modelling and Simulation in Engineering*, vol. 2018, Article ID 6524945, 13 pages, 2018.

[14] Y. Quan, F. Wang, and M. Gu, "A method for estimation of extreme values of wind pressure on buildings based on the generalized extreme-value theory," *Mathematical Problems in Engineering*, vol. 2014, Article ID 926253, 22 pages, 2014.

[15] Y. Quan, M. Gu, B. Chen, and T. Yukio, "Study on the extreme value estimating method of non-Gaussian wind pressure," *Chinese Journal of Theoretical and Applied Mechanics*, vol. 3, pp. 560–566, 2010.

[16] A. G. Davenport, "Note on the distribution of the largest value of a random function with application to gust loading," *Proceedings - Institution of Civil Engineers*, vol. 6739, no. 28, pp. 187–196, 1964.

[17] A. Kareem and J. Zhao, "Analysis of non-Gaussian surge response of tension leg platforms under wind loads," *Journal of Offshore Mechanics and Arctic Engineering*, vol. 116, no. 3, pp. 137–144, 1994.

[18] E. Simiu and J. J. Filliben, "Wind direction effects on cladding and structural loads," *Engineering Structures*, vol. 3, no. 3, pp. 181–186, 1981.

[19] F. Sadek and E. Simiu, "Peak non-Gaussian wind effects for database-assisted low-rise building design," *Journal of Engineering Mechanics*, vol. 128, no. 5, pp. 530–539, 2002.

[20] M. Kasperski and R. Hoxey, "Extreme-value analysis for observed peak pressures on the Silsoe cube," *Journal of Wind Engineering and Industrial Aerodynamics*, vol. 96, no. 6-7, pp. 994–1002, 2008.

[21] M. Kasperski, "Specification and codification of design wind loads," Habilitaion Thesis, Ruhr University Bochum, Bochum, Germany, 2000.

[22] M. Kasperski, "Design wind loads for a low-rise building taking into account directional effects," *Journal of Wind Engineering and Industrial Aerodynamics*, vol. 95, no. 9-11, pp. 1125–1144, 2007.

[23] S. M. C. Diniz, E. Simiu, and E. Simiu, "Probabilistic descriptions of wind effects and wind-load factors for database-assisted design," *Journal of Structural Engineering*, vol. 131, no. 3, pp. 507–516, 2005.

[24] S. H. Huang, Q. S. Li, and J. R. Wu, "A general inflow turbulence generator for large eddy simulation," *Journal of Wind Engineering and Industrial Aerodynamics*, vol. 98, no. 10, pp. 600–617, 2010.

[25] H. Aboshosha, A. Elshaer, G. T. Bitsuamlak, and A. E. Damatty, "Consistent inflow turbulence generator for LES evaluation of wind-induced responses for tall buildings," *Journal of Wind Engineering and Industrial Aerodynamics*, vol. 142, pp. 198–216, 2015.

[26] Z. Sh. Chen, K. T. Tse, K. C. S. Kwok, A. Kareem, and B. Kim, "Measurement of unsteady aerodynamic force on a galloping prism in a turbulent flow: a hybrid aeroelastic-pressure balance," *Journal of Fluids and Structures*, vol. 102, Article ID 103232, 2021.

[27] Z. S. Chen, H. L. Huang, Y. Xu, K. T. Tse, B. Kim, and Y. Wang, "Unsteady aerodynamics on a tapered prism under forced excitation," *Engineering Structures*, vol. 240, Article ID 112387, 2021.

[28] Z. S. Chen, X. Z. Fu, Y. Xu, C. Y. Li, B. Kim, and K. T. Tse, "A perspective on the aerodynamics and aeroelasticity of tapering: partial reattachment," *Journal of Wind Engineering and Industrial Aerodynamics*, vol. 212, Article ID 104590, 2021.

[29] C. Y. Pan and Y. H. He, *Principles and Methods of Mathematical Statistics*, Tongji University Press, Shanghai, China, 1992.